**Supplementary Information for "Electrospinning ethanol–water solutions of poly(acrylic acid): non-linear viscosity variations and sensitivity to air humidity"**

Shameek Vats, Lawrence W. Honaker, Margaret W. Frey, Francesco Basoli, and Jan P.F. Lagerwall

# A   Electrospinning set-up and conditions

Figure S1 shows a schematic of the electrospinning setup discussed in the Experimental section and used for these experiments.
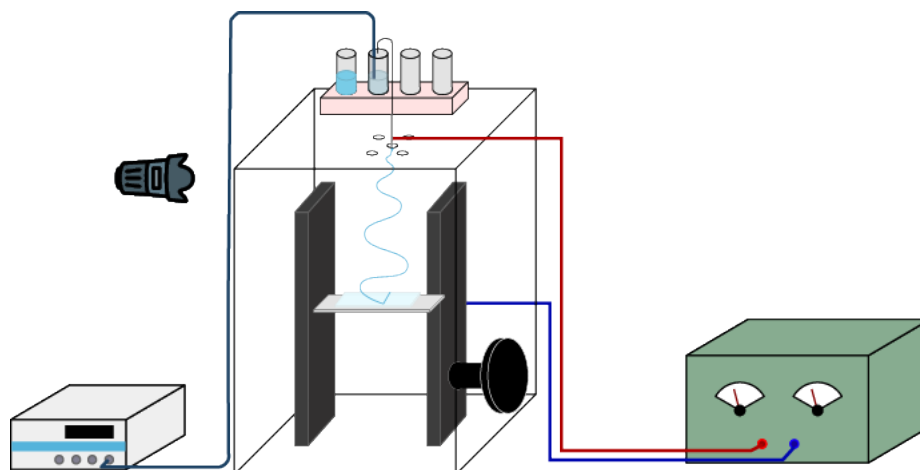


Figure S1: The schematics of the setup used for electrospinning microfibers

The parameters under which spinning took place are shown in Table S1.

Table S1: Electrospinning parameters and conditions

| PAA Concentration | Relative Humidity(%) | Temperature (°C) | Distance (cm) | Voltage (kV) | Flow rate (ml/h) |
|---|---|---|---|---|---|
| 10% w/w | 29 | 25.1 | 14 | 7.5 | 0.61 |
| 7.5% w/w | 30 | 24.8 | 14 | 7.5 | 0.65 |
| 7% w/w | 30 | 24.5 | 14 | 7.5 | 0.43 |
| 8.5% w/w | 35 | 26.3 | 14 | 7.5 | 0.23 |
| 11.5% w/w | 35 | 25.9 | 14 | 7.5 | 0.37 |

The flow rates indicated in Table S1 were calculated from the Hagen-Poiseuille equation (equation 1) for the pressure drop between two ends of a pipe or tube:

$$\Delta p = \frac{8\eta L Q}{\pi R^4} \tag{1}$$

where $\Delta p$ is the pressure difference between the ends of the tube, $Q$ the volumetric flow rate, $\eta$ the viscosity, $R$ the cross-sectional radius of the tube, and $L$ its length. Simple rearrangement allows us to express $Q$ in terms of the input parameters (most notably, $\Delta p$, $L$, and $R$):

$$Q = \frac{\Delta p \pi R^4}{8\eta L} \tag{2}$$

The parameters used in equation 2 to calculate the flow rates are indicated in Table S2.

# B   PAA solutions and their viscosities

To establish the critical entanglement concentration of our PAA in water, we replot the viscosity data from Li and Hsieh [43], obtained for the same type of PAA, in log-log scale, together with best power

| PAA concentration ($\sim$w/w) | $\eta$ (Pa·s) | R (m) $\times 10^{-4}$ | L (m) | $\Delta$ p (mbar) | Q (ml/h) |
|---|---|---|---|---|---|
| 10% | 0.86 | 4.0 | 0.343 | 50 | 0.61 |
| 7.5% | 0.65 | 4.0 | 0.343 | 40 | 0.65 |
| 7% | 0.73 | 4.0 | 0.343 | 30 | 0.43 |
| 8.5% | 0.9 | 4.0 | 0.343 | 20 | 0.23 |
| 11.5% | 0.85 | 4.0 | 0.343 | 30 | 0.37 |

Table S2: The measured values of the parameters used to calculate the flow rate.

law fits to these data, in Fig. S2. The linear character with twice the slope at high concentration suggest that $c_{PAA} \approx 5.5$ % w/w corresponds to the critical entanglement concentration.
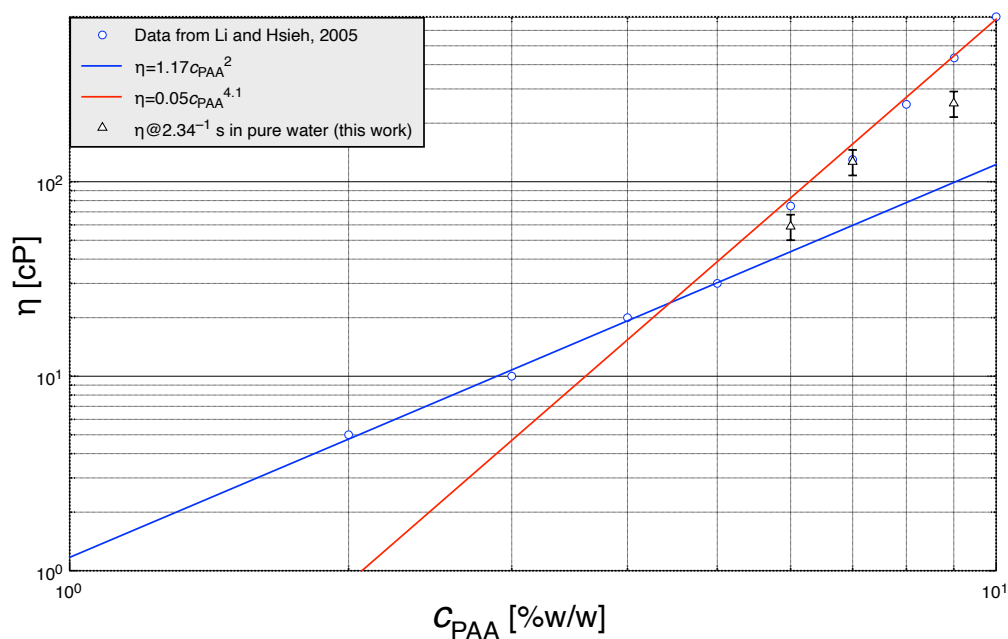


Figure S2: Log-log plot of shear viscosity $\eta$ versus PAA concentration $c_{PAA}$ in water, using experimental data extracted from Li and Hsieh [43] as well as data from this study. The two power law curves are best fits to the Li and Hsieh data at $c_{PAA} < 5.5$ % w/w and $> 5.5$ % w/w, respectively, corresponding to unentangled and entangled solution behavior. The error bars represent a standard deviation obtained from four different measurements, each with increasing and decreasing shear rate.
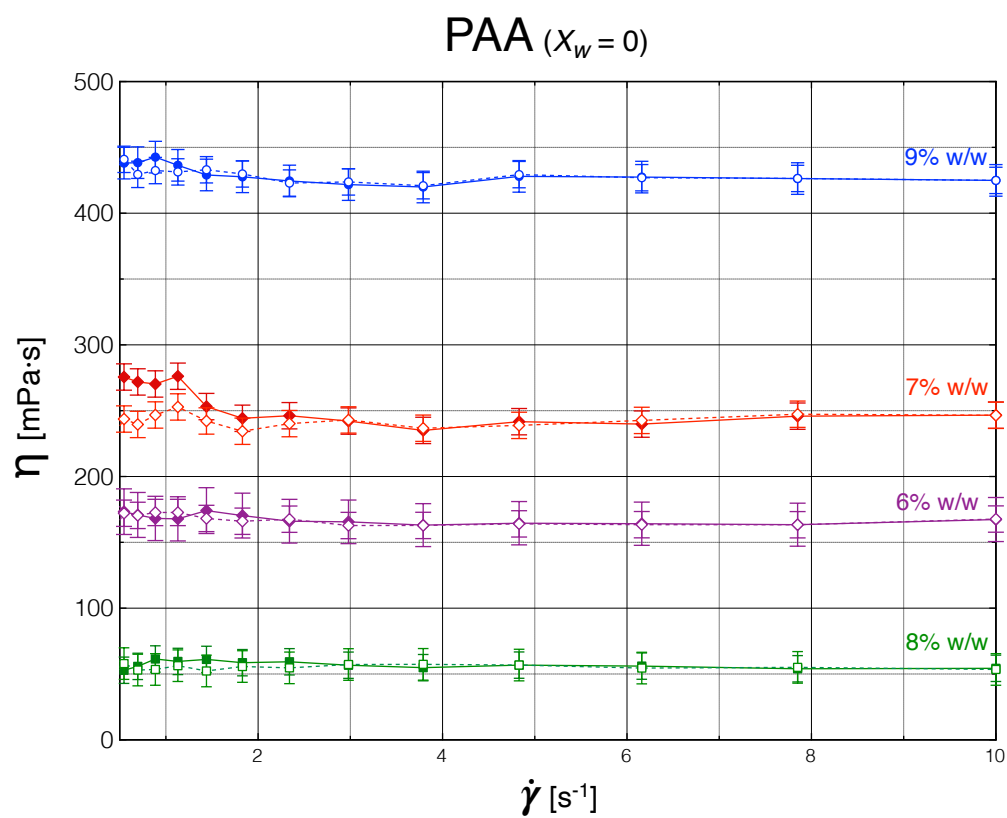
Figure S3: Viscosity $\eta$ as a function of shear rate $\dot\gamma$ for different mass concentrations $c_{PAA}$ of PAA, dissolved in pure ethanol. The error bars represent a standard deviation obtained from four different measurements, each with increasing and decreasing shear rate.
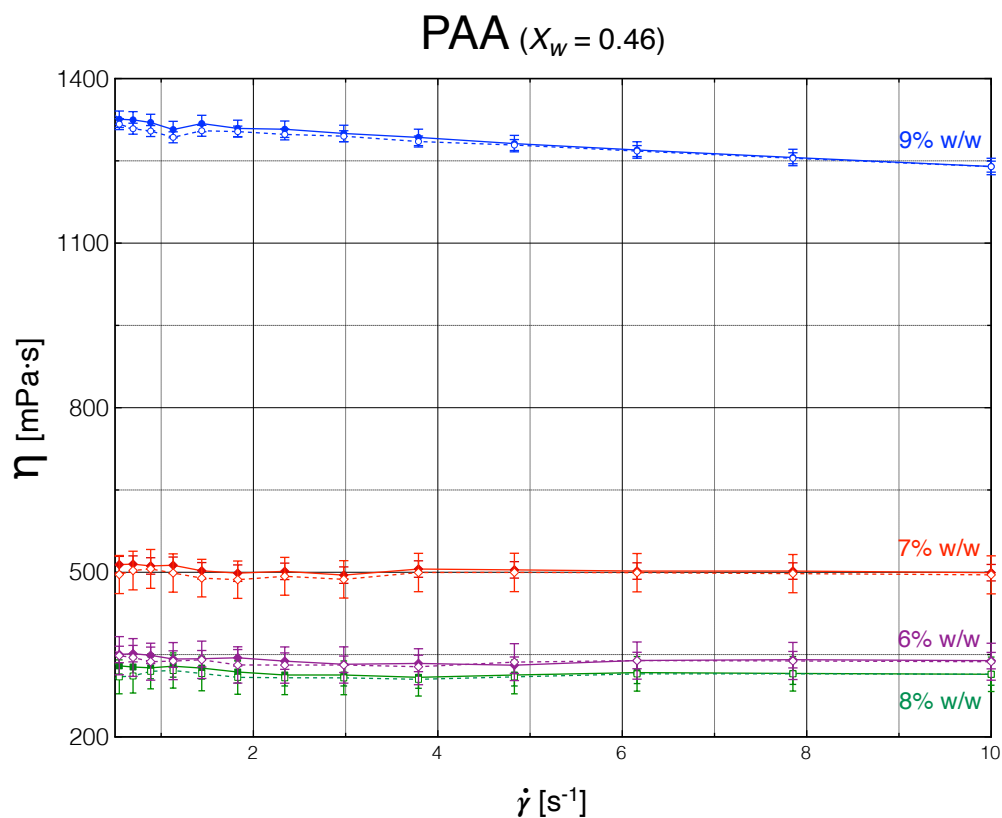
Figure S4: Viscosity $\eta$ as a function of shear rate $\dot{\gamma}$ for different mass concentrations $c_{PAA}$ of PAA, dissolved in a mixture of water and ethanol with $X_W = 0.46$. The error bars represent a standard deviation obtained from four different measurements, each with increasing and decreasing shear rate.
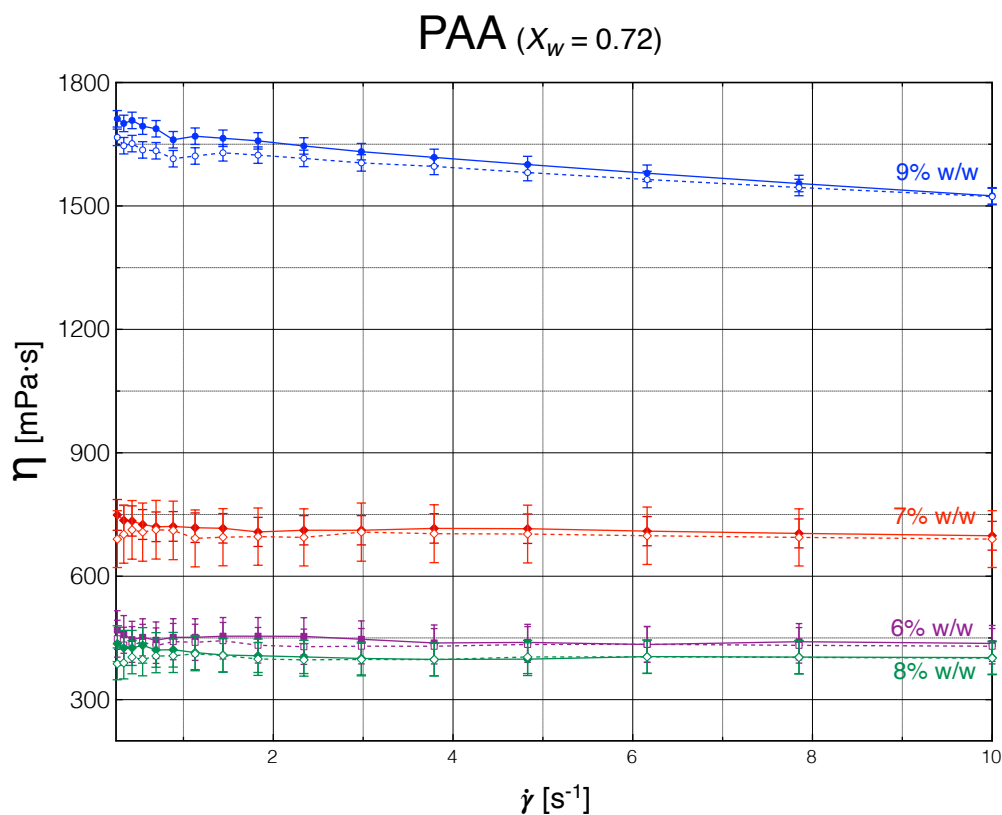


Figure S5: Viscosity $\eta$ as a function of shear rate $\dot{\gamma}$ for different mass concentrations $c_{PAA}$ of PAA, dissolved in a mixture of water and ethanol with $X_W = 0.72$. The error bars represent a standard deviation obtained from four different measurements, each with increasing and decreasing shear rate.
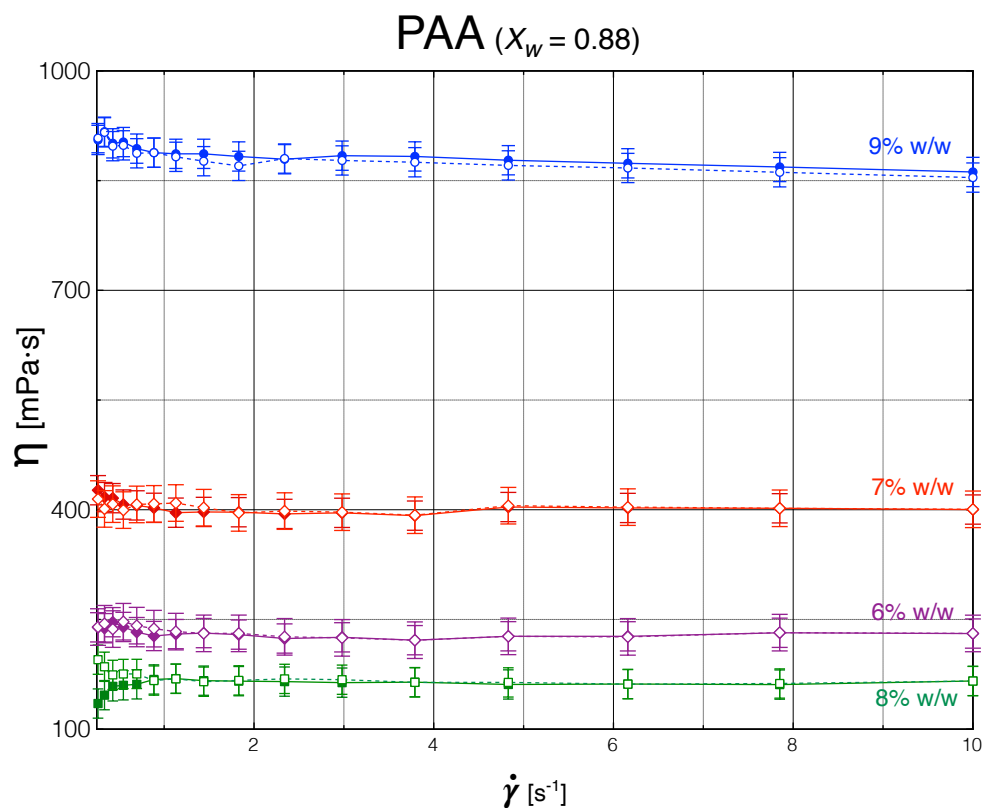
Figure S6: Viscosity $\eta$ as a function of shear rate $\dot{\gamma}$ for different mass concentrations $c_{PAA}$ of PAA, dissolved in a mixture of water and ethanol with $X_W = 0.88$. The error bars represent a standard deviation obtained from four different measurements, each with increasing and decreasing shear rate.
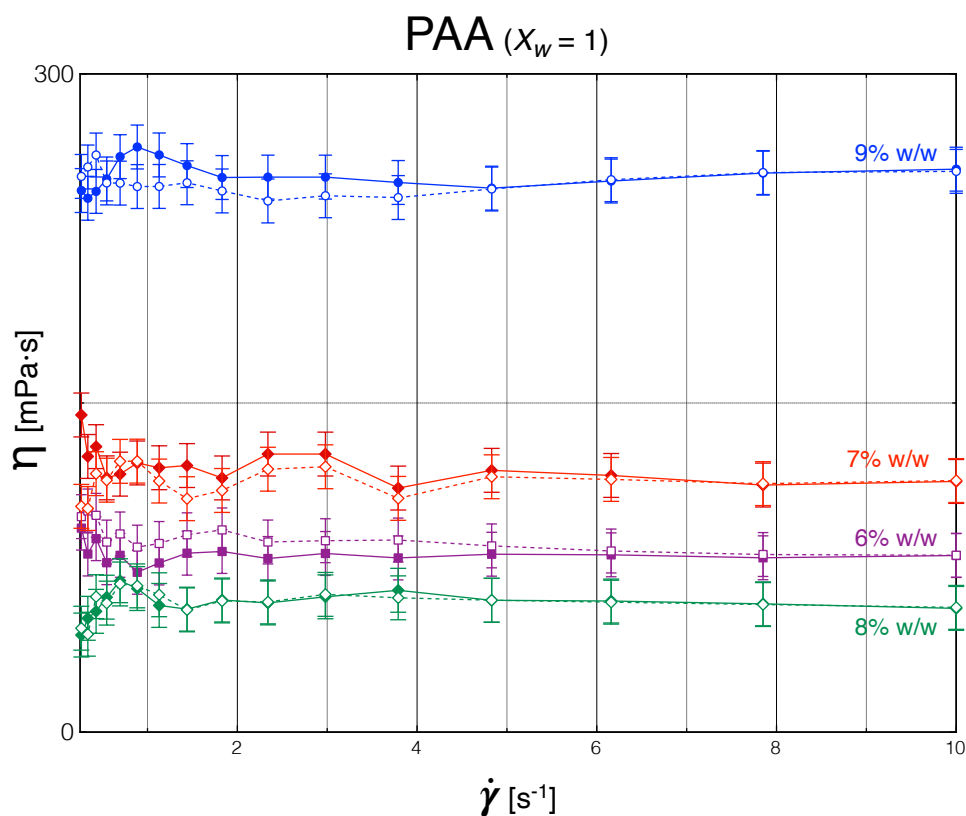


Figure S7: Viscosity $\eta$ as a function of shear rate $\dot{\gamma}$ for different mass concentrations $c_{PAA}$ of PAA, dissolved in pure water. The error bars represent a standard deviation obtained from four different measurements, each with increasing and decreasing shear rate.

# C   Anomalous 8% w/w PAA

The reason that $c_{PAA} = 8\%$ w/w is excluded from Fig. 2 in the main paper is that this concentration displayed anomalous behavior during the viscosity measurements. Throughout four attempts we could not get reproducible values, and in one attempt the instrument repeatedly produced negative $\eta$. The data at $\dot{\gamma} = 2.34$ s$^{-1}$ from all four attempts, for all five solvent compositions investigated, are shown in Fig. S8, for both increasing and decreasing shear rate $\dot{\gamma}$. We conclude that the PAA solution in this concentration range exhibits a behaviour outside the measurement conditions of the rheometer; hence we do not include them in Fig. 2. A possible reason for the anomaly may be that this particular $c_{PAA}$ range is subject to strong flow-induced phase separation by spinodal decomposition even at the rather low $\dot{\gamma}$ studied here, [62] yielding a highly inhomogeneous sample that the rheometer cannot handle. While the observation is very interesting, its proper elucidation falls outside the scope of the present work.
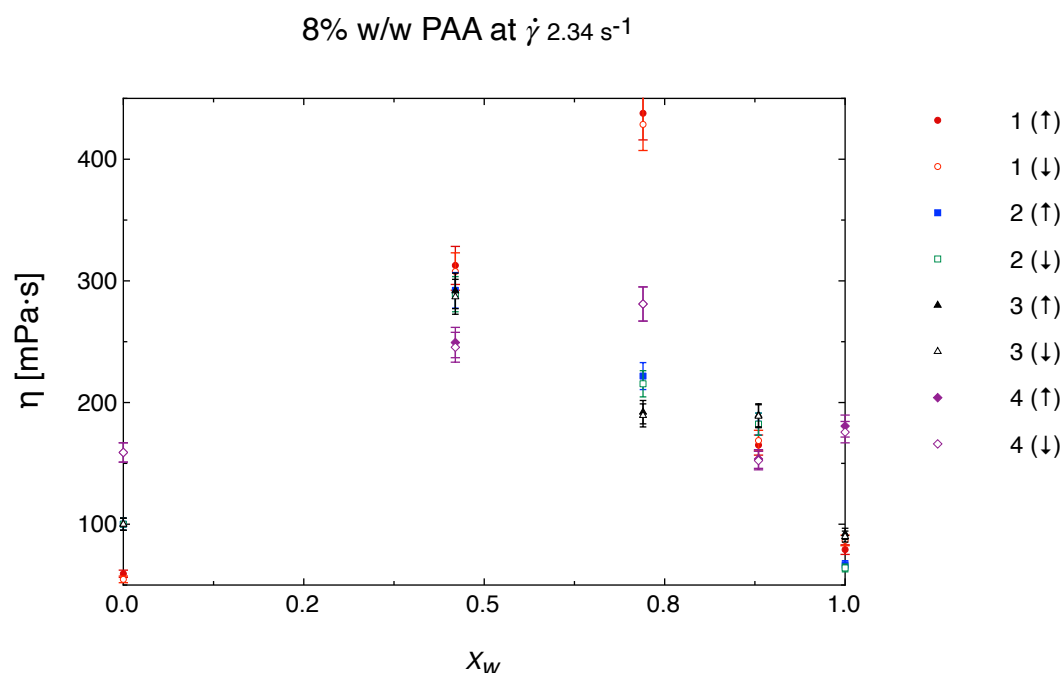


Figure S8: Rheometer output for the viscosity of 8% w/w PAA solutions at a shear rate of $\dot{\gamma} = 2.34$ s$^{-1}$, prepared with different water–ethanol ratios. The upwards arrow with solid data points shows increasing shear rate, while the downward arrow with hollowed data points show decreasing shear rate. The error bars represent the standard deviation calculated from six measurements.

# D   Viscosities of solutions optimized for electrospinning

The variation in viscosity $\eta$ at a shear rate of $\dot{\gamma}=2.34$ s$^{-1}$ for the five solutions tuned to have $\eta \approx \eta_0$, making them appropriate for electrospinning regardless of solvent composition, is shown in Fig. S9. The compositions of the solutions are summarized in Table 1 in the main paper.
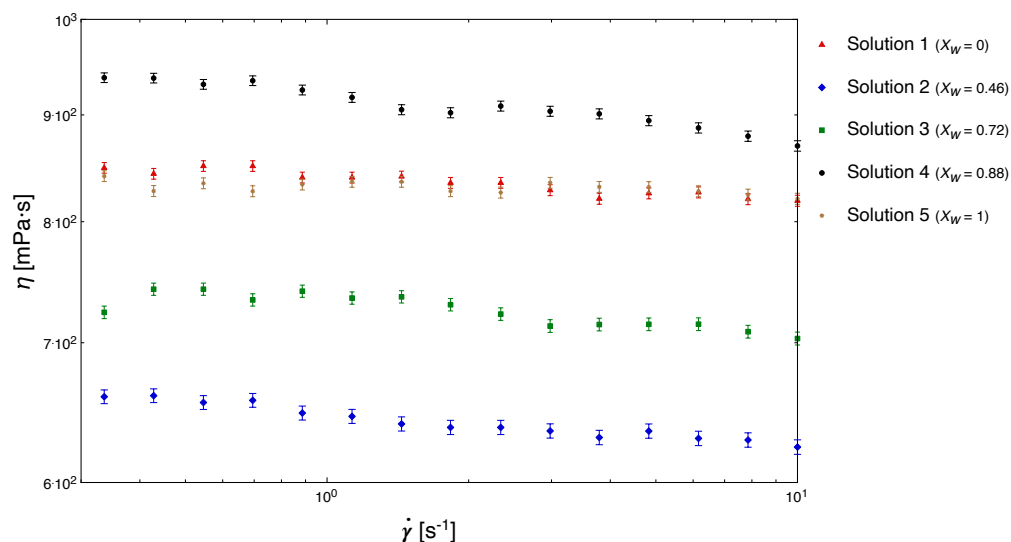
Figure S9: Log-log plot of shear viscosity ($\eta$) vs. shear rate ($\dot{\gamma}$) for the PAA solutions in Table 1, with PAA concentration $c_{PAA}$ optimized for constant viscosity regardless of water–ethanol ratio of the solvent mixture. The error bars represent a standard deviation obtained from three different measurements.

# E    pH measurements

Fresh PAA solutions of 6%, 8%, and 9% w/w were prepared for the pH measurements which were carried out using Hanna pH 211 Microprocessor pH meter at room temperature. The pH values for all the PAA concentration were measured to be lower than 5.
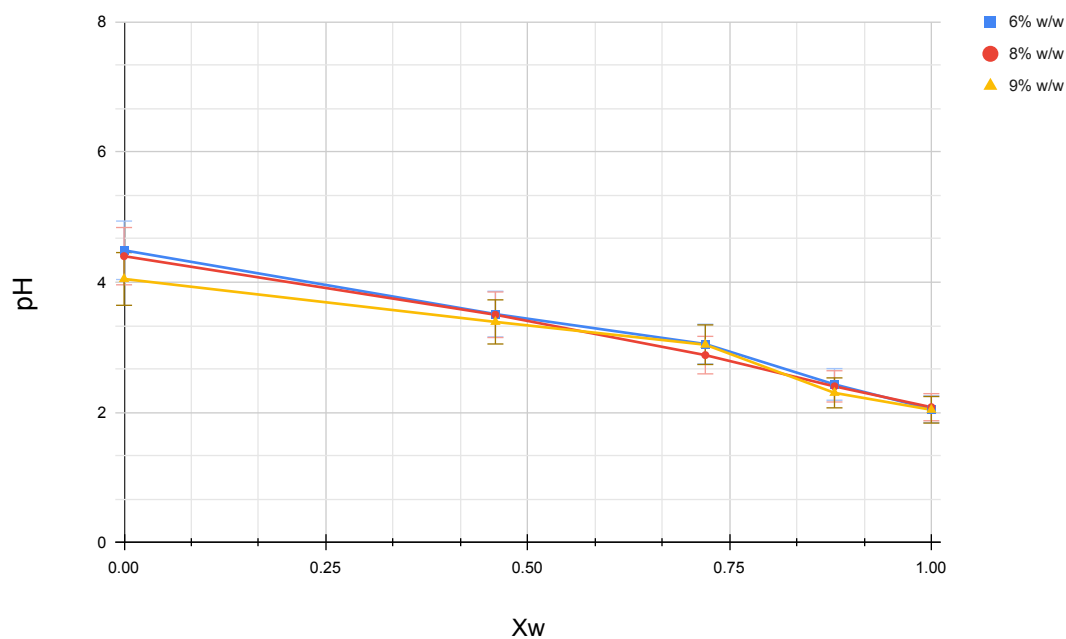


Figure S10: pH values of 6%, 8%, and 9% PAA in different mass ratios of ethanol and water. The error bars represent a standard deviation obtained from three different measurements.

# F   Visual appearance of PAA solutions with different solvent compositions

Figure S11 shows that solutions of PAA in pure water appear more turbid. As we increase the amount of ethanol in the solution, the turbidity is reduced and the solution becomes clearer (L to R). The samples were imaged after mixing for 30 s on a vortex mixer.
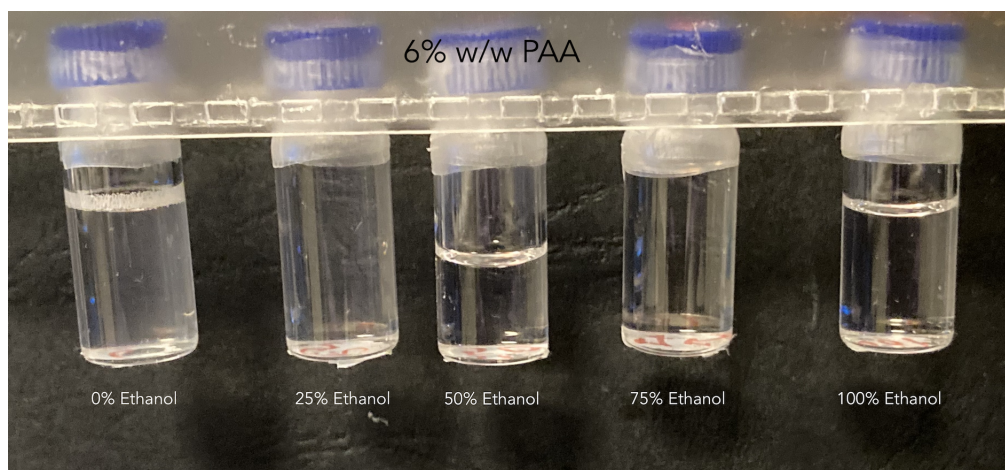


Figure S11: 6% w/w PAA solutions prepared from different ratios of ethanol and water as solvent.

# G   SI Videos

**SI movie 1**: Movie of the Taylor cone recorded during electrospinning of Solution 1 ($X_w = 0$), as listed in Table 1. The diameter of the spinneret needle is 1.20 mm and the electrospinning parameters and conditions are listed in the Table S1. This movie corresponds to Figure 3 (a) and (a').
**SI movie 2**: Movie of the Taylor cone recorded during electrospinning of Solution 2 ($X_w = 0.46$), as listed in Table 1. The diameter of the spinneret needle is 1.20 mm and the electrospinning parameters and conditions are listed in the Table S1. This movie corresponds to Figure 3 (b) and (b').
**SI movie 3**: Movie of the Taylor cone recorded during electrospinning of Solution 3 ($X_w = 0.72$), as listed in Table 1. The diameter of the spinneret needle is 1.20 mm and the electrospinning parameters and conditions are listed in the Table S1. This movie corresponds to Figure 3 (c) and (c').
**SI movie 4**: Movie of the Taylor cone recorded during electrospinning of Solution 4 ($X_w = 0.88$), as listed in Table 1. The diameter of the spinneret needle is 1.20 mm and the electrospinning parameters and conditions are listed in the Table S1. This movie corresponds to Figure 3 (d) and (d').
**SI movie 5**: Movie of the Taylor cone recorded during electrospinning of Solution 5 ($X_w = 1$), as listed in Table 1. The diameter of the spinneret needle is 1.20 mm and the electrospinning parameters and conditions are listed in the Table S1. This movie corresponds to Figure 3 (e) and (e').